

SUPER-KNEE COSMIC RAYS FROM GALACTIC NEUTRON STAR MERGER REMNANTS

SHIGEO S. KIMURA^{1,2,3}, KOHTA MURASE^{1,2,3,4}, AND PETER MÉSZÁROS^{1,2,3}

¹Department of Physics, Pennsylvania State University, University Park, Pennsylvania 16802, USA

²Department of Astronomy & Astrophysics, Pennsylvania State University, University Park, Pennsylvania 16802, USA

³Center for Particle and Gravitational Astrophysics, Pennsylvania State University, University Park, Pennsylvania 16802, USA

⁴Center for Gravitational Physics, Yukawa Institute for Theoretical Physics, Kyoto, Kyoto 606-8502, Japan

ABSTRACT

The detection of gravitational waves and electromagnetic counterparts from a binary neutron star (BNS) merger confirmed that it is accompanied by the launch of fast merger ejecta. Analogous to supernova remnants, forward shocks formed by the interaction of the ejecta with interstellar material will produce high-energy cosmic rays. We investigate the possibility that Galactic neutron star merger remnants (NSMRs) significantly contribute to the observed cosmic rays in the energy range between the knee and the ankle. Using typical parameters obtained by modeling of GW170817, we find that NSMRs can accelerate iron nuclei up to ~ 500 PeV. We calculate the cosmic-ray spectrum and composition observed on Earth, and show that the Galactic NSMR scenario can account for the experimental cosmic-ray data in the 20 – 1000 PeV range. Our model can naturally explain the hardening feature around 20 PeV for the total cosmic-ray spectrum, which has been observed by the Telescope Array Low Energy extension and the IceTop air shower array.

Keywords: cosmic rays — acceleration of particles — astroparticle physics — ISM: supernova remnants — gravitational waves — stars: neutron

1. INTRODUCTION

The origin of the diffuse cosmic-ray (CR) flux observed on Earth is one of the greatest mysteries in high-energy astrophysics. Direct-detection and air-shower experiments have revealed that the spectrum of CRs is described by a power-law function, $\Phi \propto E^{-\gamma}$ with a few break points (see, e.g., Nagano & Watson 2000; Kotera & Olinto 2011, for reviews). The first break appears around $\sim (3 - 4) \times 10^{15}$ eV (“knee”), where the spectral index changes from $\gamma \approx 2.7$ to $\gamma \approx 3.0$. A second knee appears around 10^{17} eV, above which the spectrum is softened to $\gamma \approx 3.2 - 3.3$. The third break, called the ankle, hardens the spectrum to $\gamma \approx 2.6$ around $(3 - 5) \times 10^{18}$ eV. The final break is located around 6×10^{19} eV, which is consistent with the cutoff caused by interactions with the cosmic microwave background and extragalactic background light.

Galactic supernova remnants (SNRs) are believed to be responsible for CRs below the knee (see Drury 1983; Hillas 2005; Bell 2013 for reviews). However, the recent studies of historical SNRs have indicated that the maximum energy is lower than the knee energy (see, e.g., Aharonian 2013; Ahnen et al. 2017; Abdalla et al. 2018). Different possibilities have been discussed to explain the CRs beyond the knee energy. Those include core-collapse supernovae with dense circumstellar

media (e.g., Sveshnikova 2003; Murase et al. 2014; Zirakashvili & Ptuskin 2016), the Galactic Center (Sgr A*); e.g., Abdalla et al. 2017; Fujita et al. 2017; Aharonian et al. 2018; Guépin et al. 2018), and highly spinning black holes created by binary black-hole mergers (Ioka et al. 2017). On the other hand, the CRs above the ankle, which are often called “ultrahigh-energy cosmic rays (UHECRs)”, should originate from extragalactic sources, such as active galactic nuclei (e.g., Takahara 1990; Protheroe & Szabo 1992; Berezhinsky et al. 2006; Murase et al. 2012; Fang & Murase 2018; Kimura et al. 2018b; Rodrigues et al. 2018), gamma-ray bursts (e.g., Waxman 1995; Vietri 1996; Murase et al. 2008b; Globus et al. 2015; Asano & Mészáros 2016; Biehl et al. 2018a; Zhang et al. 2018), and magnetars (e.g., Arons 2003; Murase et al. 2009; Fang et al. 2014). It seems that another component (that is often called the “B” component) is needed to fill the gap between these two components (Hillas 2005; Gaisser 2012; Gaisser et al. 2013). This second component should accelerate the CRs up to higher energies than the ordinary SNRs. This requires the combination of a higher shock velocity, a larger size, and a stronger magnetic field. The candidate sources include Galactic supernovae with dense winds (e.g., Sveshnikova 2003; Ptuskin et al. 2010; Murase et al. 2014; Zirakashvili & Ptuskin 2016), Galactic winds (Jokipii &

Morfill 1987; Völk & Zirakashvili 2004; Thoudam et al. 2016; Bustard et al. 2017; Murase & Fukugita 2018), Galactic newborn pulsars (Fang et al. 2013), Galactic gamma-ray bursts (Levinson & Eichler 1993; Wick et al. 2004; Calvez et al. 2010), trans-relativistic supernovae (Wang et al. 2007; Budnik et al. 2008), and galaxy clusters (Murase et al. 2008a; Fang & Murase 2018).

In 2017, gravitational waves from a merger of a binary neutron star (BNS) was detected, followed by the electromagnetic counterparts (Abbott et al. 2017a,b). The slowly brightening afterglow emission (e.g., Lyman et al. 2018; Mooley et al. 2018; Resmi et al. 2018; Ruan et al. 2018; Troja et al. 2018) imply the existence of relativistic jets in this system (e.g., Lazzati et al. 2017; Margutti et al. 2018), and hadronic production of high-energy neutrinos are also discussed (Kimura et al. 2017; Biehl et al. 2018b; Kimura et al. 2018a). Besides, the UV/optical/IR counterparts powered by radioactive nuclei (kilonova/macronova) enabled us to confirm that BNS mergers generate fast and massive outflows (Andreoni et al. 2017; Arcavi et al. 2017; Cowperthwaite et al. 2017; Díaz et al. 2017; Drout et al. 2017; Evans et al. 2017; Hu et al. 2017; Kasliwal et al. 2017; Lipunov et al. 2017; Pian et al. 2017; Soares-Santos et al. 2017; Utsumi et al. 2017; Valenti et al. 2017). The merger ejecta should accelerate particles at shocks formed by interaction with the interstellar material (ISM), forming a neutron star merger remnant (NSMR) analogous to an SNR. The leptonic afterglow emission of NSMRs has been intensively studied (e.g., Nakar & Piran 2011; Takami et al. 2014; Hotokezaka et al. 2016). On the other hand, the hadronic CR production was not studied in detail. Takami et al. (2014) discussed the possibility that NSMRs contribute to the CRs around the ankle, without quantitative comparisons to the experimental results. In this paper, we study the possibility that NSMRs in the Milky Way significantly contribute to the CR flux beyond the knee. The paper is organized as follows. In Section 2, we discuss CR production at typical NSMRs through the estimation of physical quantities and the maximum CR energy. In Section 3, we approximately calculate the CR spectrum and composition on Earth and compare our results to the experimental data. We discuss the related issues in Section 4 and make conclusions in Section 5. We use notations $Q_x = Q/10^x$ in CGS units otherwise noted.

2. CR PRODUCTION AT MERGER REMNANTS

2.1. Physical quantities

Theoretical modeling of GW170817 has revealed that the velocity and mass of the merger ejecta are $V_{\text{ej}} \sim 0.1c - 0.3c$ and $M_{\text{ej}} \sim 0.01 M_{\odot} - 0.05 M_{\odot}$, respectively (e.g., Kasen et al. 2017; Murguía-Berthier et al. 2017;

Rosswog et al. 2017; Smartt et al. 2017; Tanaka et al. 2017; Waxman et al. 2017; Matsumoto et al. 2018), which leads to the energy of the ejecta, $\sim 10^{50} \text{ erg} - 3 \times 10^{51} \text{ erg}$. The ejecta can consist of multiple components: a fast-light component radiating the early UV/blue photons and a slow-heavy component emitting the red/IR photons later. Since the most energetic component is likely to dominate over the other components, we approximate the ejecta as a single component. Initially, the merger ejecta freely expands into the ISM with $V_{\text{ej}} \approx V_{\text{ini}}$. After they sweep up the ISM with a mass of $\sim M_{\text{ej}}$, they start to be decelerated. The Sedov time and radius are estimated to be

$$R_{\text{dec}} \approx \left(\frac{3M_{\text{ej}}}{4\pi\mu m_p n_{\text{ISM}}} \right)^{1/3} \simeq 3.9 \times 10^{18} M_{\text{ej},-1.5}^{1/3} n_{\text{ISM},-1}^{-1/3} \text{ cm}, \quad (1)$$

$$t_{\text{dec}} \approx \frac{R_{\text{dec}}}{V_{\text{ini}}} \simeq 5.2 \times 10^8 M_{\text{ej},-1.5}^{1/3} n_{\text{ISM},-1}^{-1/3} V_{\text{ini},-0.6}^{-1} \text{ s}, \quad (2)$$

where $\mu \simeq 1.4$ is the mean molecular weight for ISM, m_p is the proton mass, n_{ISM} is the mean number density of ISM. Here, we use $M_{\text{ej},-1.5} = M_{\text{ej}}/(0.03 M_{\odot})$ and $V_{\text{ini},-0.6} = V_{\text{ini}}/(0.25c)$. For $t > t_{\text{dec}}$, the time evolution of the ejecta radius and velocity are given by the Sedov-Taylor solution: $R_{\text{ej}} \propto t^{2/5}$ and $V_{\text{ej}} \propto t^{-3/5}$, respectively.

At the forward shock of the NSMR, CRs are likely to be produced, and CR driven instabilities can amplify the magnetic field around the shock (e.g., Bell 2004). Details of the magnetic amplification at collisionless shocks are currently not well understood, so we use a simple parameterization using a constant ϵ_B parameter:

$$B \approx \sqrt{4\pi\epsilon_B\mu m_p n_{\text{ISM}} V_{\text{ej}}^2} \simeq 0.41 n_{\text{ISM},-1}^{1/2} V_{\text{ini},-0.6}^{1/2} \epsilon_{B,-3}^{1/2} \text{ mG}, \quad (3)$$

where ϵ_B is the ratio of the magnetic field pressure to the ram-pressure, and use $V_{\text{ej}} \approx V_{\text{ini}}$ at the second equation. We assume that the upstream magnetic field is also amplified to the similar value for simplicity.

2.2. Maximum energy

The maximum energy of the accelerated particles of species i , $E_{i,\text{max}}$, is determined by the balance between the acceleration and either age of the NSMR or diffusive escape time. For a quasi-parallel shock, the particle acceleration time is estimated to be (e.g., Drury 1983; Blandford & Eichler 1987)

$$t_{\text{acc}} \approx \frac{20}{3} \frac{r_{L,i}}{c} \left(\frac{V_{\text{ej}}}{c} \right)^{-2}, \quad (4)$$

where $r_{L,i} = E/(Z_i e B)$ is the Larmor radius of the particle species i (Z_i is the charge of the particle). Some fraction of the forward shock is quasi-perpendicular to the magnetic field, where the CR spectrum can be steeper than that at the quasi-parallel shocks. However, even if

we take this effect into account, the averaged spectrum is expected to be similar to that with the parallel shock for the parameter range of our interest (Bell et al. 2011).

Equating the acceleration time to the age of the NSMR, $t_{\text{age}} \approx R_{\text{ej}}/V_{\text{ej}}$, we obtain

$$E_{i,\text{max}} \approx \frac{3Z_i e B R_{\text{ej}} V_{\text{ej}}}{20c}. \quad (5)$$

The diffusive escape time from the NSMR is estimated to be $t_{\text{diff}} \approx R_{\text{ej}}^2/(2D_{\text{SNR}}) \sim R_{\text{ej}}^2/(r_{L,i}c)$, where we use $D_{\text{SNR}} \approx r_{L,i}c/3$. Then, equating the diffusion time to the acceleration time, we obtain the formula similar to equation (5). The maximum energy is proportional to t during the free-expansion phase, while $E_{i,\text{max}} \propto t^{-4/5}$ during the Sedov phase. The maximum value of $E_{i,\text{max}}$ is given at $t \sim t_{\text{dec}}$, which is estimated to be:

$$E_{i,\text{max}} \simeq 1.8 \times 10^{16} M_{\text{ej},-1.5}^{1/3} n_{\text{ISM},-1}^{1/6} V_{\text{ini},-0.6}^2 \epsilon_{B,-3}^{1/2} Z_i \text{ eV}. \quad (6)$$

Thus, the NSMRs can accelerate protons and iron nuclei to energies higher than the knee and the second knee, respectively.

2.3. Spectrum of escaping CRs

We can observe only the CRs which escape from the NSMR. The escape condition can be represented as $t_{\text{diff}} \lesssim t_{\text{age}}$. The critical energy at which $t_{\text{diff}} \sim t_{\text{age}}$ is close to that given by equation (5). Thus, low energy CRs are confined in the NSMR, and only the particles around $E_{i,\text{max}}$ can escape to ISM. Although details of the escape process are not well known, we make a brief discussion based on Ohira et al. (2010).

If the maximum energy of CRs and/or the differential CR number density, $N_{E,\text{src}}$, at the NSMR varies with time, the time integration of the escaping CRs can create a power-law spectrum. If we write $E_{i,\text{max}} \propto t^{-\alpha}$ and $N_{E,\text{src}} \propto E^{-s_{\text{inj}}} t^\beta$, the index of the escape CR spectrum is represented as $s_{\text{esc}} = s_{\text{inj}} + \beta/\alpha$ (see Appendix of Ohira et al. 2010 for applicable parameter space).

If we assume a constant CR production efficiency, the CR density can be written as $N_{E,\text{src}} \propto V_{\text{ej}}^2 R_{\text{ej}}^3$, leading to $N_{E,\text{src}} \propto t^3$ and $N_{E,\text{src}} \propto t^0$ for the free-expansion phase and the Sedov phase, respectively. Since the CR production rate is much higher during the Sedov phase, we can safely neglect the CR production during the free expansion phase. Then, we obtain $\beta \approx 0$, resulting in $s_{\text{esc}} \simeq s_{\text{inj}}$. Hence, the spectrum of escaping CRs is the same with the CRs at the source.

2.4. Composition at the source

To estimate the abundance ratio of the CRs, we use a model proposed by Caprioli et al. (2017), in which the injection efficiency for a heavy element is higher than that for protons by a factor $(A_i/Z_i)^2$ (A_i is the mass number) at the injection energy. The injection occurs

in a non-relativistic regime, and the spectral softening appears at $E \sim A_i m_p c^2$. Then, the energy density, $E^2 dN_i/dE$, of heavy element at this energy is further enhanced by another factor of $(A_i/Z_i)^{1/2}$. We assume that ISM consists of singly ionized plasma with the solar abundance ratio (see, e.g., Lodders 2003). Then, the resulting abundance ratio at the NSMR at a given energy is estimated to be $(f_p, f_{\text{He}}, f_{\text{C}}, f_{\text{O}}, f_{\text{Ne}}, f_{\text{Si}}, f_{\text{Fe}}) \simeq (0.17, 0.52, 0.024, 0.099, 0.027, 0.028, 0.14)$. The other elements are negligible. This abundance ratio is different from the abundance ratio on Earth due to propagation effects (see Section 3). The CR nuclei should be fully ionized after they are accelerated to relativistic energy.

3. CR SPECTRUM AND COMPOSITION AT EARTH

3.1. Event rate vs escape time

For NSMRs to be the sources of Galactic CRs, the occurrence time should be shorter than the CR escape time from the Galaxy. The merger rate inside our Galaxy is estimated to be $\rho_{\text{MW}} \sim \rho_{\text{mer}}/n_{\text{MW}} \sim 1.5 \times 10^{-4} \text{ yr}^{-1}$, where $\rho_{\text{mer}} \sim 1.5 \times 10^{-6} \text{ Mpc}^{-3} \text{ yr}^{-1}$ is the local BNS merger rate obtained by the GW detection (Abbott et al. 2017a) and $n_{\text{MW}} \sim 0.01 \text{ Mpc}^{-3}$ is the number density of the Milky-Way-size galaxies. This merger rate is consistent with the abundance of r-process elements in the Milky Way (Hotokezaka et al. 2018), although the rate has still large uncertainty.

The escape time of CRs from the CR halo, T_{esc} , is estimated by the abundance of radioactive nuclei (e.g., Yanasak et al. 2001; Hams et al. 2004). The value of T_{esc} depends on the details of the models. For example, leaky box models give $T_{\text{esc}} \sim 15 - 100 \text{ Myr}$ at 1 GV (Yanasak et al. 2001; Blum 2011), while diffusion halo models present longer escape timescales: $T_{\text{esc}} \sim 20 - 400 \text{ Myr}$ at 10 GV (Strong et al. 2007; Blum 2011; Lipari 2014; Yuan 2018). We often assume that $T_{\text{esc}} \propto \mathcal{R}^{-\delta}$, where $\mathcal{R} = E/(Z_i e)$ is the rigidity and $\delta \sim 0.3 - 0.6$ (Strong et al. 2007). If $\delta \lesssim 0.4$, $T_{\text{esc}} > \rho_{\text{MW}}^{-1} \sim 6.7 \times 10^3 \text{ yr}$ is always satisfied for the range of our interest ($\mathcal{R} \lesssim 10^8 \text{ GV}$). Thus, NSMRs can supply CRs before they escape from the Galaxy as long as $\delta \lesssim 0.4$. Note that this does not guarantee the homogeneity of the CRs inside the ISM. This should be examined by modeling with an inhomogeneous source distribution (see also Section 4).

Note also that we use a constant value of δ for $\mathcal{R} \lesssim 10^8 \text{ GV}$, which is not guaranteed from the experimental data. Theoretically, the resonant scattering by Kolmogorov turbulence results in $\delta \simeq 1/3$, which requires the Larmor radius of CRs to be smaller than the coherence length of interstellar turbulence. The Larmor radius for this energy range is estimated to be

$$r_{L,i} = \frac{E}{Z_i e B_{\text{ISM}}} \simeq 1.1 \times 10^{-6} \mathcal{R}_1 B_{\text{ISM},-5}^{-1} \text{ pc}, \quad (7)$$

Table 1. Model parameters used in this work.

| model | $M_{\text{ej}} [M_{\odot}]$ | $V_{\text{ej}} [c]$ | ϵ_B | $B_{\text{ISM}} [\mu\text{G}]$ | ϵ_{CR} |
|-------|-----------------------------|---------------------|--------------|--------------------------------|------------------------|
| A | 0.03 | 0.25 | 10^{-3} | — | 0.2 |
| B | 0.05 | 0.3 | — | 8 | 0.08 |

where B_{ISM} is the magnetic field in ISM and $\mathcal{R}_1 = \mathcal{R}/(10 \text{ GV})$. This can be smaller than the typical coherence length of the interstellar turbulence, $\lambda_c \sim 10 - 100 \text{ pc}$ (Han 2008). Hence, we can use the same value of δ for $\mathcal{R} \lesssim 10^8 \text{ GV}$. Also, this estimate implies that the motion of the CRs are likely diffusive rather than ballistic.

3.2. Intensity and composition

We approximate the total CR production energy per merger to be $\mathcal{E}_{\text{cr}} \approx \epsilon_{\text{cr}} M_{\text{ej}} V_{\text{ej}}^2/2$, where ϵ_{cr} is the production efficiency of CRs. We assume that the spectrum of CRs escaping from the NSMRs is a power-law with exponential cutoff: $dN_i/dE \propto E^{-s_{\text{esc}}} \exp(-E/E_{i,\text{max}})$. Then, the differential CR production rate by the NSMRs for species i is approximated to be

$$(EQ_{E,\text{inj}})_i \approx \frac{f_i \mathcal{E}_{\text{cr}} \rho_{\text{MW}}}{\ln(E_{p,\text{max}}/E_{p,\text{min}})} \exp\left(-\frac{E}{E_{i,\text{max}}}\right), \quad (8)$$

where f_i is the abundance ratio shown in Section 2.4 and we set $s_{\text{inj}} \approx s_{\text{esc}} = 2$. The normalization factor, $\ln(E_{p,\text{max}}/E_{p,\text{min}})$, is estimated by using the maximum and minimum energy for protons, and $E_{p,\text{min}}$ is set to 1 GeV.

We use the grammage to estimate the spectrum in the CR halo. The Boron-to-Carbon ratio (B/C) obtained by the recent experiments (Adriani et al. 2014; Aguilar et al. 2016) enables us to estimate the grammage traversed by CRs to be (e.g., Blum et al. 2013)

$$X_{\text{esc}} \simeq 8.7 \mathcal{R}_1^{-\delta} \text{ g cm}^{-2}. \quad (9)$$

We use $\delta = 0.46$ for $\mathcal{R} < 250 \text{ GV}$ and $\delta = 1/3$ for $\mathcal{R} \geq 250 \text{ GV}$ (Murase & Fukugita 2018). The escaping rate of CRs from the CR halo is written as $EU_E c M_{\text{gas}}/X_{\text{esc}}$, where U_E is the differential energy density of the CRs of species i and $M_{\text{gas}} \sim 10^{10} M_{\odot}$ is the gas mass inside the Milky Way galaxy. Equating the injection rate and the escape rate, we obtain (e.g., Murase & Fukugita 2018)

$$(E^2 \Phi)_i \approx \frac{(EQ_{E,\text{inj}})_i X_{\text{esc}}}{4\pi M_{\text{gas}}} \propto E^{-\delta} \exp\left(-\frac{E}{E_{i,\text{max}}}\right). \quad (10)$$

Note that the normalization of the intensity is independent of the escape time, T_{esc} , that has larger uncertainty depending on propagation models.

The resulting spectrum is shown in the upper panel of Figure 1, whose parameter set is summarized in Table 1 as model A (see Section 4 for model B). The results are almost identical to those for model A). We

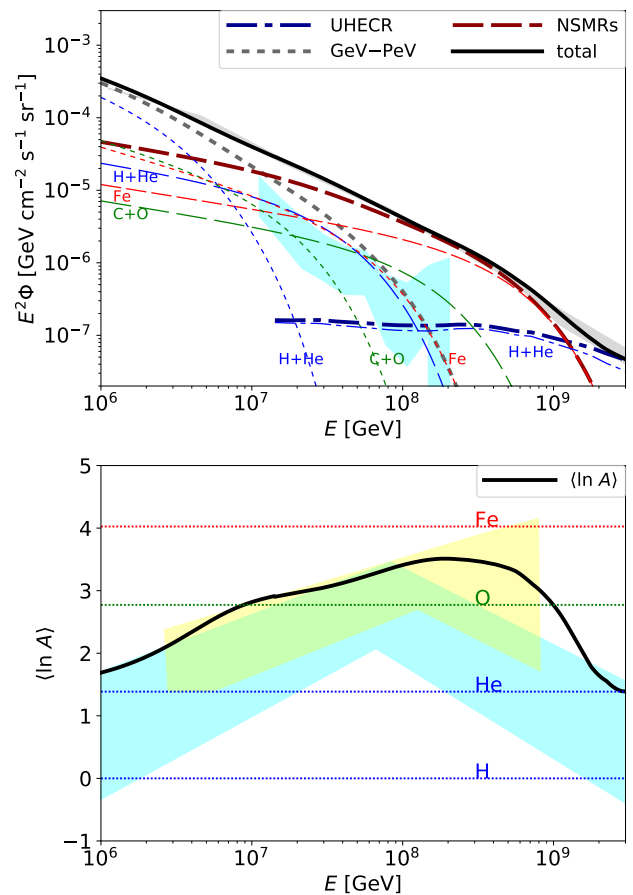


Figure 1. Upper panel: Comparison of the CR spectrum in the NSMR model to the experimental data. The thick-solid line is the total flux estimated by our model. The thick-dashed line represents the NSMRs (our work). The thick-dotted and thick-dot-dashed lines indicate the GeV–PeV and the UHECR components, respectively. See the text for the details of these components. The color-thin lines show the spectrum for each element group: H+He (blue), CNO (green), and Fe (red). The color-dashed, color-dotted, and color-dot-dashed lines are for the NSMR, the GeV–PeV, and the UHECR components, respectively. The experimental data for the total flux are taken from Verzi et al. (2017) and Abbasi et al. (2018), which are written in gray band. The flux data for the light elements (H+He) shown in the cyan region are taken from Apel et al. (2013). Lower panel: $\langle \ln A \rangle$ as a function of energy. The experimental data are taken from Kampert & Unger (2012) (cyan region) and Gaisser (2016) (yellow region). The thick-solid line is the model calculation. The parameters are set to be $n_{\text{ISM}} = 0.1 \text{ cm}^{-3}$, $\delta = 1/3$, $\rho_{\text{MW}} = 1.5 \times 10^{-4} \text{ yr}^{-1}$, $M_{\text{gas}} = 10^{10} M_{\odot}$, $s_{\text{inj}} \approx s_{\text{esc}} = 2.0$, and the other parameters are tabulated in Table 1. The results for model A and B are almost indistinguishable.

also plot two additional components, the GeV–PeV and UHECR components, which account for the regions below the knee and above the ankle, respectively. For the GeV–PeV component, the spectral shape is assumed to be a power-law and an exponential cutoff with the spectral index of -2.6 and the cutoff energy

of $2 \times 10^{15} Z_i$ eV. The abundance ratio for this component is set to be the same as that for the observed CRs at 1 TeV: $(f_p, f_{\text{He}}, f_C, f_O, f_{\text{Ne}}, f_{\text{Si}}, f_{\text{Fe}}) \simeq (0.43, 0.28, 0.052, 0.077, 0.023, 0.039, 0.10)$ (see, e.g., [Wiebel-Sooth et al. 1998](#); [Hörandel 2003](#)). We set the normalization of the GeV–PeV component so that it fits the data. For the UHECR component, we use the model by [Fang & Murase \(2018\)](#) that fits the observed UHECR data above 2×10^{18} eV as well as the ankle feature around 10^{17} eV for the CR proton and helium flux. In the range of our interest, the UHECR component is light-element dominant.

We can see that the overall spectrum is well fitted by the three components: the experimental data (gray band) is almost completely overlapped with the model curve (thick-solid line). The NSMR component is dominant for the energy range 2×10^{16} eV – 10^{18} eV. This causes a slight hardening for the total flux at $E \sim 2 \times 10^{16}$ eV, which is consistent with the recent experiments ([Aartsen et al. 2013](#); [Abbasi et al. 2018](#)).

The abundance ratio of the CRs from the NSMRs on Earth is $(f_p, f_{\text{He}}, f_C, f_O, f_{\text{Ne}}, f_{\text{Si}}, f_{\text{Fe}}) \simeq (0.10, 0.41, 0.028, 0.13, 0.037, 0.043, 0.26)$. This helium abundance is higher than that for the GeV–PeV component. This arises from the injection prescription with the assumption of a singly ionized plasma (see [Section 2.4](#)). The ionization degree in the ISM could be higher, which suppresses the CR nuclei production compare to CR protons. Also, majority of heavy elements exist in dust grains, which enhances the injection efficiency of the heavy elements ([Ellison et al. 1997](#)). These effects can decrease the helium abundance. Detailed modeling including these effects are beyond the scope of this paper.

Our model is also in good agreement with the spectrum for the light elements (H + He), which show a hardening around 10^{17} eV ([Apel et al. 2013](#); [Buitink et al. 2016](#)). The light elements from the NSMRs match the observed spectrum below the hardening, and the UHECR component accounts for the energy range above the hardening. The contribution from the GeV–PeV component is negligible there because of the lower cut-off energy. The bottom panel shows the average mass number, $\langle \ln A \rangle$. This is also consistent with the experimental results, although they have large uncertainty.

4. DISCUSSION

We use a simple assumption about the magnetic field amplification using a constant ϵ_B parameter, which is widely used to discuss the afterglow emission of gamma-ray bursts and NSMRs ([Mészáros 2006](#); [Kumar & Zhang 2015](#)). Recent particle simulations ([Caprioli & Spitkovsky 2014](#); [van Marle et al. 2018](#)) suggest that the magnetic field amplification at non-relativistic shocks is

represented as

$$B \sim \sqrt{0.5 \mathcal{M}_A} B_{\text{ISM}} \simeq 0.25 V_{\text{ini}, -0.6}^{1/2} n_{\text{ISM}, -1}^{1/4} B_{\text{ISM}, -5}^{1/2} \text{ mG}, \quad (11)$$

where $\mathcal{M}_A = V_{\text{ej}}/V_A$ is the Alfvén mach number and $V_A = B_{\text{ISM}}/\sqrt{4\pi\mu m_p n_{\text{ISM}}}$ is the Alfvén velocity at the upstream. Even using this formalism of magnetic field amplification, our model can explain the CRs around the second knee with an optimistic set of parameters tabulated in [Table 1](#) as model B. The resulting spectrum and composition are almost identical to those shown in [Figure 1](#).

Although we set the spectrum index at the source to $s_{\text{inj}} = 2$, it could be softer. It is widely believed that Galactic SNRs accelerate the CRs below the knee, where the spectral index at the Earth is $\gamma \approx 2.7 - 2.8$. This results in the spectral index at the sources, $s_{\text{esc}} \approx 2.4$ ([Murase & Fukugita 2018](#)). The spectral softening can be caused by a number of reasons (e.g., [Ohira & Ioka 2011](#)). A softer escape spectrum requires a higher CR production rate to achieve the observed CR intensity. Since we use a fairly high value of ϵ_{CR} for model A, this might cause some tension between our model and experimental data.

When BNSs merge, faster ejecta can be dynamically produced due to the shock formed by the merger. This dynamical ejecta can be faster ($\beta_{\text{ej}} = V_{\text{ej}}/c \lesssim 0.8$) and lighter ($M_{\text{ej}} \sim 0.01 M_{\odot}$). According to the afterglow observations of GW170817, the kinetic energy distribution of the dynamical ejecta can be $\mathcal{E}_k(> \Gamma_{\text{ej}} \beta_{\text{ej}}) \propto (\Gamma_{\text{ej}} \beta_{\text{ej}})^{-5}$ ([Mooley et al. 2018](#)). With this steep profile, the slower shell accelerates CRs to higher energy than the faster shell, because the faster shell is decelerated too quickly to accelerate CRs. Thus, we can neglect the CRs produced by the fast tail of the dynamical ejecta.

CRs are produced also at reverse shocks of the NSMRs. Since the merger ejecta consist of r -process elements, these CRs should be heavier than iron. However, the CR experiments around GeV energy suggest that there is no strong enhancement of r -process elements ([Binns et al. 1989](#); [Donnelly et al. 2012](#)), which limits the CR production efficiency at the reverse shocks of NSMRs to be lower than 3×10^{-5} ([Kyutoku & Ioka 2016](#)). In our model, the CRs produced at the reverse shock should be confined inside the ejecta, and are expected to lose energies by adiabatic expansion so that the r -process elements do not have to contribute to the observed CRs.

The central remnant object left after a BNS merger could be a magnetar. In this case, it produces the magnetar wind with the total energy $\mathcal{E}_w \sim 10^{52}$ erg if the rotation period is ~ 1 ms (e.g., [Yu et al. 2013](#); [Metzger & Piro 2014](#); [Murase et al. 2018](#)). The energy and mass of the wind are deposited to the ejecta of the merger,

so the ejecta of NSMRs can be faster and more massive than those we assumed in this paper, leading to mildly relativistic ejecta. This kind of energetic ejecta can produce higher-energy CRs, so the production of UHECRs is possible. If one third of BNS mergers have magnetars left, and 30 % of ejecta energy is spent to produce CRs, the luminosity density for UHECR production at $E \sim 10^{19}$ eV is roughly estimated to be $\mathcal{C}\epsilon_{\text{cr}}\mathcal{E}_w\rho_{\text{mer}}/3 \sim 10^{44}$ erg Mpc $^{-3}$ yr $^{-1}$, where $\mathcal{C} \sim 1/15$ is the bolometric correction factor. This value is consistent with the required luminosity density of observed UHECRs (e.g., [Katz et al. 2009](#); [Murase & Takami 2009](#)). Note that the central remnant of GW170817 should be a black hole, because we do not observe the luminous X rays and high-energy gamma rays in later time from GW170817 (see [Murase et al. 2018](#) for related discussions). The magnetar model will be examined by the counterpart searches of GWs (see [Abbott et al. 2017b](#), and references therein) and transient searches in the radio band ([Hales 2013](#); [Bhattacharyya et al. 2016](#); [Fender et al. 2017](#)).

The heavy elements might be disintegrated by interaction with photons during the propagation in ISM. For iron nuclei with energy $\sim 10^{18}$ eV, the target photons for the giant dipole resonance is $E_\gamma \sim 1$ eV. The energy density of infrared radiation field is ~ 1 eV cm $^{-3}$, leading to the photon number density $n_\gamma \sim 1$ cm $^{-3}$. The photo-disintegration timescale is then $t_{A\gamma} \sim (n_\gamma\sigma_{A\gamma}c)^{-1} \sim 10$ Myr, where $\sigma_{A\gamma} \sim 10^{-25}$ cm 2 is the giant dipole resonant cross-section for iron nuclei. Although this is sufficiently longer than the escape time of CRs of $E_{\text{Fe}} \sim 10^{18}$ eV, the radiation density is much higher in the Galactic Center, where the CR nuclei would be destroyed. The detailed simulation including this effect is beyond the scope of this paper. Note that since the CRs are produced during the Sedov phase ($t_{\text{dec}} \gtrsim 10$ years), we safely neglect the disintegration at the NSMR. Also, the spallation by interaction with ISM is not important in this energy range.

The NSMRs can be located above the Galactic disk because of the natal kick. The spacial distribution of NSMRs is likely to be similar to the distribution of millisecond pulsars ([Lorimer 2013](#)) and X-ray binaries ([Repetto et al. 2017](#)). The scale height of the CR halo, H_h , is often set to be 4 kpc – 6 kpc (e.g., [Strong et al. 2007](#)), which is larger than the distributions of these objects. Hence, the Galactic BNS mergers are likely to occur inside this CR halo. Then, the NSMRs intermittently inject the CRs at random positions in the CR halo, which results in an inhomogeneous CR distribution. This causes the dipole anisotropy. The dipole anisotropy of CRs from the isotropically distributed sources in the disk is roughly estimated to be (e.g., [Blasi](#)

& [Amato 2012a](#))

$$a \sim \frac{D}{cH_h} \sim 1.7 \times 10^{-4} \mathcal{R}_1^\delta H_{h,22.2}, \quad (12)$$

where D is the diffusion coefficient and we set $H_h \sim 5$ kpc and $D \sim 8 \times 10^{28} \mathcal{R}_1^\delta$ cm 2 s $^{-1}$. For 10^{16} eV $< E < 10^{18}$ eV, CR arrival direction is almost isotropic and upper limits for the amplitude of dipole anisotropy are ~ 0.01 ([Antoni et al. 2004](#); [The Pierre Auger Collaboration et al. 2015](#)). Our rough estimate results in $a \sim$ a few percents for $\mathcal{R} \sim 10^8$ GV, which might have a tension with the observations. However, NSMRs can be located above the Galactic disk, so the estimate above is not appropriate in our situation. The realistic value of a should be calculated by solving the anisotropic diffusion equations, appropriately taking into account magnetic field geometry and intermittent and inhomogeneous CR sources (see e.g., [Blasi & Amato 2012b](#); [Pohl & Eichler 2013](#); [Mertsch & Funk 2015](#), for lower energy CRs).

Mergers of neutron star-black hole (NS-BH) binaries are also expected to produce energetic outflows ([Ross-wog 2005](#); [East et al. 2012](#); [Foucart et al. 2014](#); [Kiuchi et al. 2015](#); [Kyutoku et al. 2015](#)), which is likely to produce CRs as is the case with BNS mergers. The numerical simulations indicate that NS-BH mergers can produce more energetic outflows than those by BNS mergers ([Just et al. 2015](#); [Wu et al. 2016](#)). Although the NS-BH merger rate and its ejecta energy is more uncertain at present, the planned GW experiments and counterpart searches will reveal the physical quantities in the system near future.

5. SUMMARY

We have investigated the CR production due to Galactic NSMRs, based on the parameters estimated from the observations of GW170817. Assuming efficient amplification of the magnetic field at forward shocks, we have found that the NSMRs can accelerate protons and iron nuclei up to 2×10^{16} eV and 5×10^{17} eV, respectively. The event rate of BNS mergers is high enough to provide CRs before they escape from the Galaxy. Using a simple model that takes into account the escape process during the Sedov phase and the enhancement of heavy elements in the CR injection, we have calculated the spectrum and composition of the CRs on Earth. Together with the GeV-PeV CR and UHECR components, our model can be consistent with the observed CR data. The NSMR component may give a significant contribution to the CR flux at energies of 10^{16} eV $\lesssim E \lesssim 10^{18}$ eV, and the other components should account for the CRs below the knee and above the ankle. Our model could also match the spectrum for the light elements (H and He) around 10^{16} eV $\lesssim E \lesssim 3 \times 10^{17}$ eV.

S.S.K thanks Susumu Inoue for useful discussion at the ASJ annual meeting on March 2018. We are grateful to Kunihito Ioka for helpful comments and Ke Fang for providing the data. This work is supported by JSPS Oversea Research Fellowship, the IGC post-doctoral fellowship program (S.S.K.), Alfred P. Sloan Foundation, NSF Grant No. PHY-1620777 (K.M.), and NASA

NNX13AH50G (P.M.). While we were finalizing this project, we became aware of a related but independent work by Rodrigues et al. (arXiv:1806.01624). They focus on extragalactic BNS mergers and CR protons around the ankle, whereas we concentrate on the Galactic NSMRs and CR irons around and beyond the second knee.

REFERENCES

- Aartsen, M. G. et al. 2013, *PhRvD*, 88, 042004, 1307.3795
- Abbasi, R. U. et al. 2018, *ArXiv e-prints*, 1803.01288
- Abbott, B. P. et al. 2017a, *Physical Review Letters*, 119, 161101, 1710.05832
- . 2017b, *ApJL*, 848, L12, 1710.05833
- Abdalla, H. et al. 2017, *ApJL*, 850, L22, 1710.05862
- Abdalla, H., et al. 2018, *Astron. Astrophys.*, 612, A6, 1609.08671
- Adriani, O. et al. 2014, *ApJ*, 791, 93, 1407.1657
- Aguilar, M. et al. 2016, *Physical Review Letters*, 117, 231102
- Aharonian, F., Yang, R., & de Oña Wilhelmi, E. 2018, *ArXiv e-prints*, 1804.02331
- Aharonian, F. A. 2013, *Astroparticle Physics*, 43, 71
- Ahnen, M. L., et al. 2017, *Mon. Not. Roy. Astron. Soc.*, 472, 2956, 1707.01583, [Erratum: *Mon. Not. Roy. Astron. Soc.* 476, no.3, 2874 (2018)]
- Andreoni, I., Ackley, K., Cooke, J., Acharyya, A., & et al. 2017, *PASA*, 34, e069, 1710.05846
- Antoni, T. et al. 2004, *ApJ*, 604, 687, astro-ph/0312375
- Apel, W. D. et al. 2013, *Astroparticle Physics*, 47, 54
- Arcavi, I. et al. 2017, *ApJL*, 848, L33, 1710.05842
- Arons, J. 2003, *ApJ*, 589, 871, astro-ph/0208444
- Asano, K., & Mészáros, P. 2016, *PhRvD*, 94, 023005, 1607.00732
- Bell, A. R. 2004, *MNRAS*, 353, 550
- . 2013, *Astroparticle Physics*, 43, 56
- Bell, A. R., Schure, K. M., & Reville, B. 2011, *MNRAS*, 418, 1208, 1108.0582
- Berezinsky, V., Gazizov, A., & Grigorieva, S. 2006, *PhRvD*, 74, 043005, hep-ph/0204357
- Bhattacharyya, B. et al. 2016, *ApJ*, 817, 130, 1509.07177
- Biehl, D., Boncioli, D., Fedynitch, A., & Winter, W. 2018a, *A&A*, 611, A101, 1705.08909
- Biehl, D., Heinze, J., & Winter, W. 2018b, *MNRAS*, 476, 1191, 1712.00449
- Binns, W. R. et al. 1989, *ApJ*, 346, 997
- Blandford, R., & Eichler, D. 1987, *PhR*, 154, 1
- Blasi, P., & Amato, E. 2012a, *JCAP*, 1, 010, 1105.4521
- . 2012b, *JCAP*, 1, 011, 1105.4529
- Blum, K. 2011, *JCAP*, 11, 037, 1010.2836
- Blum, K., Katz, B., & Waxman, E. 2013, *Physical Review Letters*, 111, 211101, 1305.1324
- Budnik, R., Katz, B., MacFadyen, A., & Waxman, E. 2008, *ApJ*, 673, 928, 0705.0041
- Buitink, S. et al. 2016, *Nature*, 531, 70, 1603.01594
- Bustard, C., Zweibel, E. G., & Cotter, C. 2017, *ApJ*, 835, 72, 1610.06565
- Calvez, A., Kusenko, A., & Nagataki, S. 2010, *Physical Review Letters*, 105, 091101, 1004.2535
- Caprioli, D., & Spitkovsky, A. 2014, *ApJ*, 794, 46, 1401.7679
- Caprioli, D., Yi, D. T., & Spitkovsky, A. 2017, *Physical Review Letters*, 119, 171101, 1704.08252
- Cowperthwaite, P. S., Berger, E., Villar, V. A., Metzger, B. D., Nicholl, M., Chornock, R., Blanchard, P. K., & et al. 2017, *ApJL*, 848, L17, 1710.05840
- Díaz, M. C., Macri, L. M., Garcia Lambas, D., & et al. 2017, *ApJL*, 848, L29, 1710.05844
- Donnelly, J., Thompson, A., O’Sullivan, D., Daly, J., Drury, L., Domingo, V., & Wenzel, K.-P. 2012, *ApJ*, 747, 40
- Drout, M. R., Piro, A. L., Shappee, B. J., Kilpatrick, C. D., & et al. 2017, *Science*, 358, 1570, 1710.05443
- Drury, L. O. 1983, *Reports on Progress in Physics*, 46, 973
- East, W. E., Pretorius, F., & Stephens, B. C. 2012, *PhRvD*, 85, 124009, 1111.3055
- Ellison, D. C., Drury, L. O., & Meyer, J.-P. 1997, *ApJ*, 487, 197, astro-ph/9704293
- Evans, P. A., Cenko, S. B., Kennea, J. A., Emery, S. W. K., & et al. 2017, *Science*, 358, 1565, 1710.05437
- Fang, K., Kotera, K., Murase, K., & Olinto, A. V. 2014, *PhRvD*, 90, 103005, 1311.2044
- Fang, K., Kotera, K., & Olinto, A. V. 2013, *JCAP*, 3, 010, 1302.4482
- Fang, K., & Murase, K. 2018, *Nature Physics*, 14, 396, 1704.00015
- Fender, R., Woudt, P. A., Armstrong, R., Groot, P., & et al. 2017, *ArXiv e-prints*, 1711.04132
- Foucart, F. et al. 2014, *PhRvD*, 90, 024026, 1405.1121
- Fujita, Y., Murase, K., & Kimura, S. S. 2017, *JCAP*, 4, 037, 1604.00003
- Gaisser, T. K. 2012, *Astroparticle Physics*, 35, 801, 1111.6675
- Gaisser, T. K. 2016, *Nucl. Part. Phys. Proc.*, 279-281, 47, 1601.06670
- Gaisser, T. K., Stanev, T., & Tilav, S. 2013, *Frontiers of Physics*, 8, 748, 1303.3565
- Globus, N., Allard, D., Mochkovitch, R., & Parizot, E. 2015, *MNRAS*, 451, 751, 1409.1271
- Guépin, C., Rinchiuso, L., Kotera, K., Moulin, E., Pierog, T., & Silk, J. 2018, *ArXiv e-prints*, 1806.03307
- Hales, C. A. 2013, *ArXiv e-prints*, 1312.4602
- Hams, T. et al. 2004, *ApJ*, 611, 892
- Han, J. L. 2008, *Nuclear Physics B Proceedings Supplements*, 175, 62, 0901.0040
- Hillas, A. M. 2005, *Journal of Physics G Nuclear Physics*, 31, R95
- Hörandel, J. R. 2003, *Astroparticle Physics*, 19, 193, astro-ph/0210453
- Hotokezaka, K., Beniamini, P., & Piran, T. 2018, *ArXiv e-prints*, 1801.01141
- Hotokezaka, K., Nissanke, S., Hallinan, G., Lazio, T. J. W., Nakar, E., & Piran, T. 2016, *ApJ*, 831, 190, 1605.09395
- Hu, L., Wu, X., Andreoni, I., Ashley, M. C. B., & et al. 2017, *Science Bulletin*, Vol. 62, No.21, p.1433-1438, 2017, 62, 1433, 1710.05462
- Ioka, K., Matsumoto, T., Teraki, Y., Kashiyama, K., & Murase, K. 2017, *MNRAS*, 470, 3332, 1612.03913
- Jokipii, J. R., & Morfill, G. 1987, *ApJ*, 312, 170
- Just, O., Bauswein, A., Ardevol Pulpillo, R., Goriely, S., & Janka, H.-T. 2015, *MNRAS*, 448, 541, 1406.2687

- Kampert, K.-H., & Unger, M. 2012, *Astroparticle Physics*, 35, 660, 1201.0018
- Kasen, D., Metzger, B., Barnes, J., Quataert, E., & Ramirez-Ruiz, E. 2017, *Nature*, 551, 80, 1710.05463
- Kasliwal, M. M., Nakar, E., Singer, L. P., Kaplan, D. L., & et al. 2017, *Science*, 358, 1559, 1710.05436
- Katz, B., Budnik, R., & Waxman, E. 2009, *JCAP*, 3, 020, 0811.3759
- Kimura, S. S., Murase, K., Bartos, I., Ioka, K., Heng, I. S., & Mészáros, P. 2018a, *ArXiv e-prints*, 1805.11613
- Kimura, S. S., Murase, K., Mészáros, P., & Kiuchi, K. 2017, *ApJL*, 848, L4, 1708.07075
- Kimura, S. S., Murase, K., & Zhang, B. T. 2018b, *PhRvD*, 97, 023026, 1705.05027
- Kiuchi, K., Sekiguchi, Y., Kyutoku, K., Shibata, M., Taniguchi, K., & Wada, T. 2015, *PhRvD*, 92, 064034, 1506.06811
- Kotera, K., & Olinto, A. V. 2011, *ARA&A*, 49, 119, 1101.4256
- Kumar, P., & Zhang, B. 2015, *PhR*, 561, 1, 1410.0679
- Kyutoku, K., & Ioka, K. 2016, *ApJ*, 827, 83, 1603.00467
- Kyutoku, K., Ioka, K., Okawa, H., Shibata, M., & Taniguchi, K. 2015, *PhRvD*, 92, 044028, 1502.05402
- Lazzati, D., Perna, R., Morsony, B. J., López-Cámara, D., Cantiello, M., Ciolfi, R., giacomazzo, B., & Workman, J. C. 2017, *ArXiv e-prints*, 1712.03237
- Levinson, A., & Eichler, D. 1993, *ApJ*, 418, 386
- Lipari, P. 2014, *ArXiv e-prints*, 1407.5223
- Lipunov, V. M., Gorbvskoy, E., Kornilov, V. G., & et al. 2017, *ApJL*, 850, L1, 1710.05461
- Lodders, K. 2003, *ApJ*, 591, 1220
- Lorimer, D. R. 2013, in *IAU Symposium*, Vol. 291, *Neutron Stars and Pulsars: Challenges and Opportunities after 80 years*, ed. J. van Leeuwen, 237–242, 1210.2746
- Lyman, J. D., Lamb, G. P., Levan, A. J., Mandel, I., & et al. 2018, *ArXiv e-prints*, 1801.02669
- Margutti, R. et al. 2018, *ArXiv e-prints*, 1801.03531
- Matsumoto, T., Ioka, K., Kisaka, S., & Nakar, E. 2018, *ArXiv e-prints*, 1802.07732
- Mertsch, P., & Funk, S. 2015, *Physical Review Letters*, 114, 021101, 1408.3630
- Mészáros, P. 2006, *Reports on Progress in Physics*, 69, 2259, astro-ph/0605208
- Metzger, B. D., & Piro, A. L. 2014, *MNRAS*, 439, 3916, 1311.1519
- Mooley, K. P., Nakar, E., Hotokezaka, K., Hallinan, G., & et al. 2018, *Nature*, 554, 207, 1711.11573
- Murase, K., Dermer, C. D., Takami, H., & Migliori, G. 2012, *Astrophys. J.*, 749, 63, 1107.5576
- Murase, K., & Fukugita, M. 2018, *ArXiv e-prints*, 1806.04194
- Murase, K., Inoue, S., & Nagataki, S. 2008a, *ApJL*, 689, L105, 0805.0104
- Murase, K., Ioka, K., Nagataki, S., & Nakamura, T. 2008b, *PhRvD*, 78, 023005, 0801.2861
- Murase, K., Mészáros, P., & Zhang, B. 2009, *PhRvD*, 79, 103001, 0904.2509
- Murase, K., & Takami, H. 2009, *ApJL*, 690, L14, 0810.1813
- Murase, K., Thompson, T. A., & Ofek, E. O. 2014, *MNRAS*, 440, 2528, 1311.6778
- Murase, K. et al. 2018, *ApJ*, 854, 60, 1710.10757
- Murguía-Berthier, A. et al. 2017, *ApJL*, 848, L34, 1710.05453
- Nagano, M., & Watson, A. A. 2000, *Reviews of Modern Physics*, 72, 689
- Nakar, E., & Piran, T. 2011, *Nature*, 478, 82, 1102.1020
- Ohira, Y., & Ioka, K. 2011, *ApJL*, 729, L13
- Ohira, Y., Murase, K., & Yamazaki, R. 2010, *A&A*, 513, A17, 0910.3449
- Pian, E., D’Avanzo, P., Benetti, S., Branchesi, M., & et al. 2017, *Nature*, 551, 67, 1710.05858
- Pohl, M., & Eichler, D. 2013, *ApJ*, 766, 4, 1208.5338
- Protheroe, R. J., & Szabo, A. P. 1992, *Physical Review Letters*, 69, 2885
- Ptuskin, V., Zirakashvili, V., & Seo, E.-S. 2010, *ApJ*, 718, 31, 1006.0034
- Repetto, S., Igoshev, A. P., & Nelemans, G. 2017, *MNRAS*, 467, 298, 1701.01347
- Resmi, L. et al. 2018, *ArXiv e-prints*, 1803.02768
- Rodrigues, X., Fedynitch, A., Gao, S., Boncioli, D., & Winter, W. 2018, *ApJ*, 854, 54, 1711.02091
- Rosswog, S. 2005, *ApJ*, 634, 1202, astro-ph/0508138
- Rosswog, S., Sollerman, J., Feindt, U., Goobar, A., Korobkin, O., Fremling, C., & Kasliwal, M. 2017, *ArXiv e-prints*, 1710.05445
- Ruan, J. J., Nynka, M., Haggard, D., Kalogera, V., & Evans, P. 2018, *ApJL*, 853, L4, 1712.02809
- Smartt, S. J., Chen, T.-W., Jerkstrand, A., Coughlin, M., & et al. 2017, *Nature*, 551, 75, 1710.05841
- Soares-Santos, M., Holz, D. E., Annis, J., Chornock, R., & et al. 2017, *ApJL*, 848, L16, 1710.05459
- Strong, A. W., Moskalenko, I. V., & Ptuskin, V. S. 2007, *Annual Review of Nuclear and Particle Science*, 57, 285, astro-ph/0701517
- Sveshnikova, L. G. 2003, *A&A*, 409, 799, astro-ph/0303159
- Takahara, F. 1990, *Progress of Theoretical Physics*, 83, 1071
- Takami, H., Kyutoku, K., & Ioka, K. 2014, *PhRvD*, 89, 063006, 1307.6805
- Tanaka, M., Utsumi, Y., Mazzali, P. A., Tominaga, N., & et al. 2017, *PASJ*, 69, 102, 1710.05850
- The Pierre Auger Collaboration et al. 2015, *ArXiv e-prints*, 1509.03732
- Thoudam, S., Rachen, J. P., van Vliet, A., Achterberg, A., Buitink, S., Falcke, H., & Hörandel, J. R. 2016, *A&A*, 595, A33, 1605.03111
- Troja, E. et al. 2018, *ArXiv e-prints*, 1801.06516
- Utsumi, Y., Tanaka, M., Tominaga, N., Yoshida, M., & et al. 2017, *PASJ*, 69, 101, 1710.05848
- Valenti, S. et al. 2017, *ApJL*, 848, L24, 1710.05854
- van Marle, A. J., Casse, F., & Marcowith, A. 2018, *MNRAS*, 473, 3394, 1709.08482
- Verzi, V., Ivanov, D., & Tsunesada, Y. 2017, *ArXiv e-prints*, 1705.09111
- Vietri, M. 1996, *MNRAS*, 278, L1, astro-ph/9510148
- Völk, H. J., & Zirakashvili, V. N. 2004, *A&A*, 417, 807, astro-ph/0401368
- Wang, X.-Y., Razzaque, S., Mészáros, P., & Dai, Z.-G. 2007, *PhRvD*, 76, 083009, 0705.0027
- Waxman, E. 1995, *Physical Review Letters*, 75, 386, astro-ph/9505082
- Waxman, E., Ofek, E., Kushnir, D., & Gal-Yam, A. 2017, *ArXiv e-prints*, 1711.09638
- Wick, S. D., Dermer, C. D., & Atoyan, A. 2004, *Astroparticle Physics*, 21, 125, astro-ph/0310667
- Wiebel-Sooth, B., Biermann, P. L., & Meyer, H. 1998, *A&A*, 330, 389, astro-ph/9709253
- Wu, M.-R., Fernández, R., Martínez-Pinedo, G., & Metzger, B. D. 2016, *MNRAS*, 463, 2323, 1607.05290
- Yanasak, N. E. et al. 2001, *ApJ*, 563, 768
- Yu, Y.-W., Zhang, B., & Gao, H. 2013, *ApJL*, 776, L40, 1308.0876
- Yuan, Q. 2018, *ArXiv e-prints*, 1805.10649
- Zhang, B. T., Murase, K., Kimura, S. S., Horiuchi, S., & Mészáros, P. 2018, *PhRvD*, 97, 083010, 1712.09984
- Zirakashvili, V. N., & Ptuskin, V. S. 2016, *Astroparticle Physics*, 78, 28, 1510.08387